Linking synoptic forcing and local mesoscale processes with biological dynamics off Ningaloo Reef

Vincent Rossi,[1] Ming Feng,[2] Charitha Pattiaratchi,[3] Moninya Roughan,[1] and Anya M. Waite[3]

Received 23 July 2012; revised 5 February 2013; accepted 5 February 2013; published 14 March 2013.

[1] A hydrographic survey offshore Ningaloo reef, north-west Australia, in austral autumn 2010 revealed relatively stable subsurface water masses in the region, despite the influence of interannual variability of the Leeuwin Current (LC). The surface water mass seems slightly more variable at seasonal time scale, probably due to various contributions of the geographically distinct source waters of the LC. A subsurface nitrate maximum (~110–230 m), a prominent feature of the Ningaloo area during autumn, was consistently observed within different water masses. Tightly coupled variations of subsurface nitrate and oxygen at small vertical scale suggest it is due to local in situ remineralization of organic matter likely to accumulate along sharp physical interfaces and possibly favored by injections of oxygenated subsurface waters. Offshore, enhanced levels of surface chlorophyll *a* within the downwelling-favorable LC are associated with deeper mixed layer depth, eroding the shallow source of nutrients. Close to the continental shelf, these nutrients are observed to be efficiently uplifted within the core of quasi-persistent topographically trapped submesoscale cyclonic eddies dominated by nonlinear effects. A wind-driven coastal upwelling event occurred in autumn and was characterized by a relatively deep source (~100–150 m), coinciding with the subsurface maximum of nutrients, thus promoting coastal productivity locally and farther north by alongshore advection within the Ningaloo current.

Citation: Rossi, V., M. Feng, C. Pattiaratchi, M. Roughan and A. M. Waite (2013), Linking synoptic forcing and local mesoscale processes with biological dynamics off Ningaloo Reef, *J. Geophys. Res. Oceans. 118*, 1211–1225, doi:10.1002/jgrc.20110.

1. Introduction

[2] Surface circulation in the south eastern Indian Ocean off north Western Australia (NWA) is dominated by the Leeuwin Current system that consists of the near surface flow, the southward Leeuwin Current (LC), the deeper northward flow of the Leeuwin Undercurrent (LU), and transient coastal countercurrents (the Ningaloo Current, NC) [*Cresswell and Golding*, 1980; *Thompson*, 1987; *Woo et al*., 2006a, 2006b; *Woo and Pattiaratchi*, 2008; *Pattiaratchi and Woo*, 2009]. This atypical eastern boundary current (LC) is forced by an alongshore pressure gradient that inhibits the development of large-scale upwelling, resulting in the transport of warmer, lower-salinity tropical waters poleward [*Thompson*, 1987; *Smith et al*., 1991; *Pattiaratchi and Woo*, 2009]. Seasonally, maximum poleward flow by the LC is reached during the austral autumn-winter (May–July) as indicated by coastal sea level variability and historical hydrographic surveys [*Feng et al*., 2003]. There is a distinct interannual variability associated with the El Niño–Southern Oscillation (ENSO) index, the volume transport of the LC being greater during La Niña years than during El Niño years [*Feng et al*., 2008].

[3] More specifically, the LC forms as a well-defined surface current at the latitudes north of Northwest Cape, off the Gascoyne shelf (20°S –23°S). This area is thus crucial for the regional oceanography, as it constitutes a topographic funnel where the LC consolidates from several branches originating from both the Eastern Tropical Indian Ocean and the Indonesian Throughflow (Pacific Ocean waters) [*Domingues et al*., 2007]. Although it constitutes the initiation of a coherent LC, this complex and dynamical oceanic region has not been sampled in great detail to date. Farther south, the LC consists of a relatively narrow, shallow but intense current flowing over the upper continental slope along the WA coast up to Cape Leeuwin (35°S) and even farther [*Ridgway and Condie*, 2004]. The eddy kinetic energy of the LC is substantially higher than that of other

[1]School of Mathematics and Statistics, The University of New South Wales, Sydney, New South Wales, Australia.
[2]CSIRO Marine and Atmospheric Research, Floreat, Western Australia, Australia.
[3]School of Environmental Systems Engineering and the Oceans Institute, The University of Western Australia, Crawley, Western Australia, Australia.

Corresponding author: V. Rossi, School of Mathematics and Statistics, The University of New South Wales, Sydney, NSW 2052, Australia. (vincent.rossi.ocean@gmail.com)

2169-9275/13/10.1002/jgrc.20110

eastern boundary currents [*Feng et al*., 2005], resulting in meanders and eddies spinning up everywhere along the WA coast [*Feng et al*., 2007; *Rennie et al*., 2007; *Meuleners et al*., 2007]. In particular, complex recirculating flows have been repeatedly observed over the extended shelf in the vicinity of Point Cloates (~22.75°S) [*Taylor and Pearce*, 1999; *Woo et al*., 2006a].

[4] The Ningaloo offshore region is characterized by seasonally nitrate-depleted surface waters which are often high in silicate [*Lourey et al*., 2006] and low primary production concentrated at a deep chlorophyll maximum (DCM) [*Hanson et al*., 2005]. The variability of the biological productivity off Ningaloo reef appears to be controlled by processes occurring at different spatiotemporal scales, including regional scale forcing and more localized shelf-scale processes. *Koslow et al*. [2008] documented a large-scale autumn bloom, extending offshore the whole WA coast including the Ningaloo region. This major seasonal event which concerned the whole surface layers coincides with the initial intensification of the LC. Several potential sources for this seasonal influx of nutrients off the WA coast have been proposed, such as eddy-induced horizontal transport of nutrients from the coast [*Waite et al*., 2007; *Moore et al*., 2007], nitrogen fixation [*Twomey et al*., 2007], and seasonal cooling associated with a deepening of the mixed layer deep (MLD) [*Rousseaux et al*., 2012]. Another hypothesis for the autumn bloom is the entrainment of a low dissolved oxygen/high nitrate (LDOHN) layer [*Woo and Pattiaratchi*, 2008; *Thompson et al*., 2011]. These relatively shallow and elevated nitrate concentrations, possibly originating from nitrification [*Paterson et al*., 2008; *Thompson et al*., 2011], were hypothesized to fuel the shelf-scale autumn bloom. However, the origins of the particulate organic matter acting as a substrate of the nitrification processes remain unclear, and both local and remote sources have been suggested, a topic which is explored in more detail by *Waite et al*. [2013].

[5] More localized enrichment processes are driven by sporadic wind-driven upwelling events which occur primarily during the austral summer (December–March) [*Thompson*, 1987; *Weaver and Middleton*, 1989]. These upwelling-favorable (northward) winds have also been associated with a system of equatorward coastal countercurrents inshore of the LC as the Ningaloo Current (NC) that extends along the NWA coast [*Taylor and Pearce*, 1999; *Hanson et al*., 2005; *Woo and Pattiaratchi*, 2008]. The combination of these wind-driven coastal currents and localized inner shelf upwelling seasonally restricts the inshore extent of the LC and has been related with somewhat higher biological productivity [*Hanson et al*., 2005, *Hanson and McKinnon*, 2009]. *Twomey et al*. [2007] also documented evidence of a positive phytoplankton response to a subsurface upwelling off Perth, despite the local nitrate concentrations remaining undetectable. Although persistent upwelling does not prevail in the LC system, sporadic upwelling events have been observed along the Gascoyne shelf only in the summer season [*Hanson et al*., 2005; *Woo et al*., 2006a]. Recently, based on moored time series off the Ningaloo Peninsula, *Lowe et al*. [2012] showed that upwelling seemed not limited to summer periods without depicting precisely the oceanic response and its biological impact.

[6] Based on a multidisciplinary data set collected off the Gascoyne coast in May 2010, we first describe the regional scale oceanographic context observed during the survey and we discuss the current hypothesis related to the autumn bloom. Supported by further analysis of the data set, we then focus on smaller-scale coastal processes that resulted in local nutrient enrichment and associated biological response. It includes quasi-persistent topographically trapped submesoscale eddies and two consecutive wind-driven upwelling events. Finally, we discuss our results in the context of existing work, and we conclude with an analysis of the interactions between small-scale and large-scale biophysical processes off the NWA region.

2. Materials and Methods

2.1. Study Area and Sampling Strategy

[7] The multidisciplinary research voyage onboard the R/V *Southern Surveyor* (SS04-2010) was focused on a 2° by 2° area off north-west Australia, where the LC is defined to originate. This area (~21°S–23°S/113°E–115°E) was intensively surveyed through seven cross-shelf transects from north to south at about every half a degree of latitude from 10 to 20 May 2010 (Figure 1). Each transect extended from the 50–2000 m isobaths, with major sampling stations set at specific depth contours, where a suite of physical and biological measurements were undertaken.

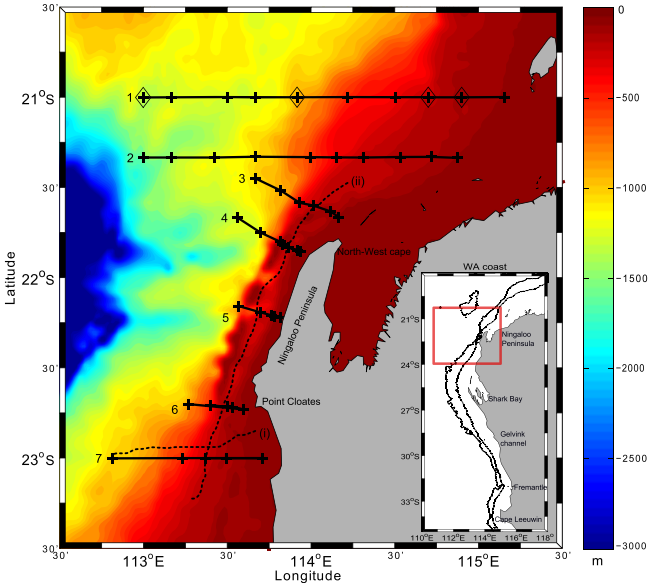

Figure 1. Overview of the survey off the Ningaloo Peninsula. Black crosses indicate the CTD stations as cross-shelf sections (numbered from 1 at 21°S to 7 at 23°S), black dotted line (i & ii) represent the Nacelle towed body trajectories, superimposed on the coloured bathymetry. The diamonds along line 1 indicate the location of release of the drifters. A map of Western Australia is displayed on the lower right insert (thin black lines indicate the 200 and 1000 m isobaths) with the area of study highlighted by the red rectangle.

2.2. Cruise Data and Analysis

[8] Observations were made using a conductivity-temperature-depth (CTD) probe and a set of biogeochemical as well as optical sensors mounted onto the CTD-Rosette. In this paper, we used data from a Chelsea Aqua 3 fluorometer (chlorophyll *a*), from a SBE43 oxygen sensor, and from an In Situ Ultraviolet Spectrophotometer (ISUS) nitrate sensor, all lowered on the Rosette.

[9] More than 100 CTD casts were performed during the cruise (see Figure 1), composed of around 50 casts using only the CTD-Rosette system and around 80 casts including water sampling using the CTD-Rosette-Niskin system (equipped with twelve 10 L Niskin bottles), spread out along the seven cross-shelf transects from 21°S to 23°S. At each station, up to five depths in the water column were sampled during the upcast: the surface (1 m), the upper thermocline, the deep chlorophyll maximum, the lower thermocline, and an additional depth of interest. The CTD casts off the narrow Ningaloo shelf were performed up to 1000 m, whereas the nearshore profiles were restricted to at least 10 m above the shallow topography.

[10] In addition, a nacelle towed body ("tow-yo" instrument) was used during each transit between transects, thus providing high-resolution CTD data for the top 200 m at a vertical resolution of 1 m. The horizontal spacing of each dive varied within 1–4 km, depending on the velocity of the ship.

[11] The dissolved oxygen probe mounted on the rosette was calibrated by independent sampling spread over the whole campaign to cover different biogeochemical environments. The correlation between the dissolved oxygen concentrations from the Winkler titrations [*Labasque et al.*, 2004] and from the CTD probe is very good ($R^2 = 0.97$), and the factor of the linear regression is 1. The apparent oxygen utilization (AOU) was computed according to *Garcia and Gordon* [1992] as the difference between the saturation value (that depends on the corresponding temperature and salinity) and the measured dissolved oxygen.

[12] Dissolved inorganic nutrients (nitrate + nitrite, hereafter nitrate, phosphate, and silicate) were analyzed for all depths using a shipboard Autoanalyzer. Detection limits were 0.1 µmol/L for nitrate and silicate and 0.01 µmol/L for phosphate. All the nitrate concentrations derived from bottle measurements during the whole cruise were used to calibrate the ISUS sensor ($R^2 = 0.95$)

[13] For total chlorophyll *a* analysis, 1 L samples were filtered onto Whatman GF/F filters and stored frozen until extraction in 8 ml 90% acetone within 3 days of collection. For analysis of the >5 µm fraction, 2 L of seawater were filtered onto 5 µm Nitex mesh. All samples were analyzed for chlorophyll *a* with a fluorometer without grinding. Samples were acidified with 10% HCl to correct for phaeopigments, and chlorophyll *a* concentrations were calculated according to *Parsons et al.* [1984]. This extracted chlorophyll *a* data were used to convert fluorescence into chlorophyll *a* values in mg/m^3. The values of total chlorophyll *a* are obtained by using the best fitted linear model: [chlo-*a*] $\simeq 0.032$ * fluorescence $- 0.49$ ($R^2 = 0.65$). Total chlorophyll *a* concentrations and small to large (> 5 µm) cell ratio are used in the following.

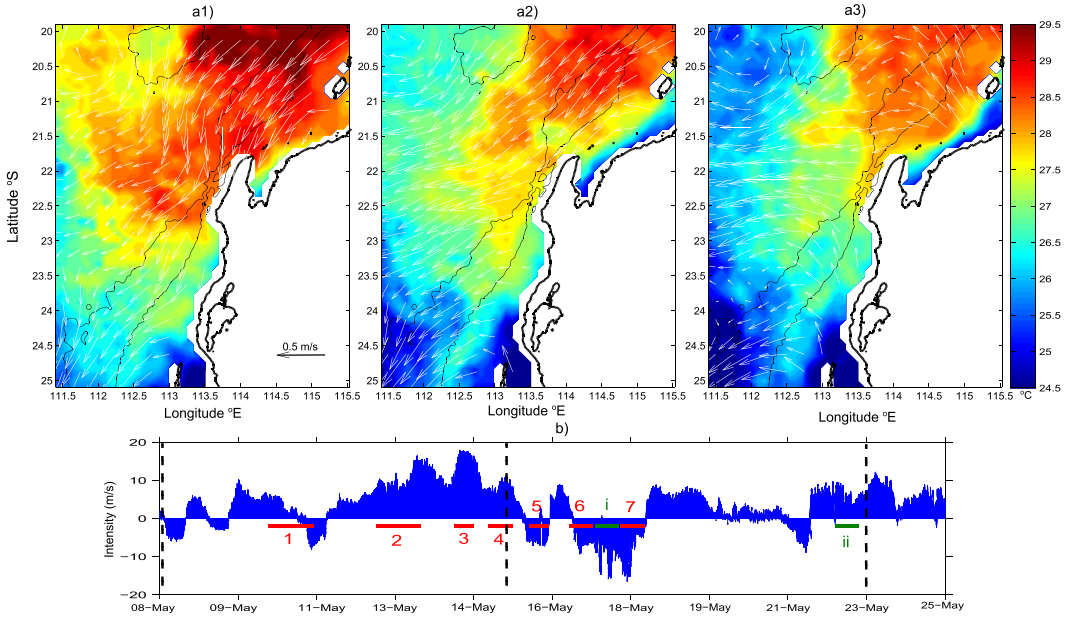

Figure 2. Oceanographic context during the survey. Sea surface temperature snapshots and surface currents (derived from satellite (J. Sudre et al., On the global estimates of Q5 geostrophic and Ekman surface currents, submitted to *Limnology and Oceanography: Fluids and Environments*, 2012) superimposed on (a1) 8 May, (a2) 15 May, and (a3) 23 May 2010. Black thin lines indicate the 200 and 1000 m isobaths. (b) Onboard measured winds (m/s) for the duration of the field survey. Red/green segments indicate when the respective sections were performed. Black dashed lines indicate the corresponding date of snapshots (a1)–(a3). The wind vectors emanate from equally spaced points along the horizontal *x* axis, while the vector components are expressed relative to the origin of the respective vector. The vectors pointing up represent a wind blowing northward of intensity directly readable on the *y* axis.

[14] Continuous underway measurements of the horizontal current velocity along the ship's track was obtained using a vessel-mounted RDI 75 kHz Broadband Acoustic Doppler Current Profiler (ADCP), 8 m depth bins through the water column from about 20 to 400 m. Meteorological conditions (e.g., wind speed and direction) were also measured simultaneously by shipboard instrumentation during the voyage (see Figure 2b). All continuous vertical profiles coming from the CTD sensors were 1 m binned. Both CTD and ADCP data presented in this paper were plotted using an optimal elliptic interpolation.

[15] The Brunt-Väisälä frequency, N^2, was computed on each profile using the following equation:

$$N^2 = -\frac{g\partial\rho}{\rho_0\partial z} \quad (1)$$

where N^2 is in rad^2/s^2, ρ_0 is a reference potential density (mean of the vertical profile), ρ is the potential density, g is the acceleration due to gravity, and z is the depth. Each vertical profile was smoothed using a moving average over five indices ($\simeq$5 m) to filter out small-scale structure and noise.

2.3. Remotely Sensed Data

[16] Remote sensing products, including sea surface temperature (SST) and surface total currents, are used to provide synoptic views of the surface ocean. Daily snapshots of cloud-free SST data are obtained through the optimally interpolated SST product at 1/10° (about 10 km) resolution from the Remote Sensing Systems (NASA/NOAA). Because of the through-cloud capabilities of microwave radiometers, it provides a valuable picture of cloud-free SST over the Western Australian coast. Surface total currents (displayed on Figures 2a1–2a3) are a combination of both Geostrophic and Ekman currents derived from altimetry and scatterometry, respectively. More details about this product can be found in J. Sudre et al. (submitted manuscript, 2012).

3. Results

3.1. Oceanographic and Meteorological Context

[17] Meteorological data recorded onboard the R/V *Southern Surveyor* were in good agreement with those measured from the land-based weather station, although the coastal winds are slightly underestimating the wind observed further offshore (not shown). Winds were variable and relatively weak (<10 m/s) before and during the first part of the campaign until 12 May 2010 (Figure 2b). After this date, upwelling-favorable (southerly, e.g., northward) winds dominated, with two main events, up to 18 m/s from 12 to 16 May and after a short wind reversal, northward winds commenced again from 18 to 24 May at speeds of up to 12 m/s.

[18] There was initially a strong LC as shown by the warm waters (>28°C) flowing southward before 12 May 2010 (Figure 2a1). After the first upwelling-favorable/northward wind event (15 May, Figure 2a2), a general cooling (26°C–27°C) of the surface waters off Ningaloo was observed, probably due to coastal upwelling and strong wind mixing, from winds opposing the main southward LC. The surface currents derived from altimetry and scatterometry [*Sudre et al.*, 2012] gradually weakened and turned southwestward. On 23 May (Figure 2a3), their direction had completely shifted westward (offshore), driven by the Ekman forces (northward wind). These conditions led to a localized coastal upwelling with relatively colder water (temperature around 24°C–25°C within the 100 m isobath north and south of Ningaloo Peninsula) spreading over the continental shelf and apparently flowing northward. Note

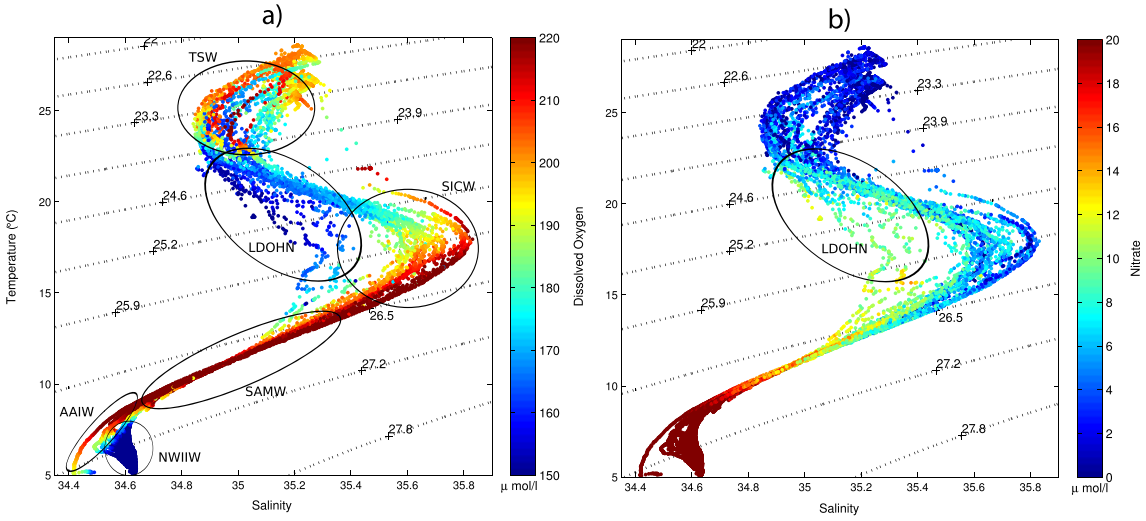

Figure 3. Water mass analysis. Potential temperature versus absolute salinity diagram for the whole campaign using 2 m binned data. Each measurement has been colored according to (a) its dissolved oxygen content (in μmol/L, from the oxygen probe) and (b) its nitrate content (in μmol/L). Annotations indicate the main water masses: Tropical Surface Water (TSW), Low Dissolved Oxygen/High Nitrate layer (LDOHN), South Indian Central Waters (SICW), Sub-Antarctic Mode Water (SAMW), Antarctic Intermediate Water (AAIW), and North West Indian Intermediate Water (NWIIW).

the altimeter data do not resolve fully the narrow coastal current.

[19] We observed a transition from stratified LC-dominated conditions to mixed conditions associated with coastal upwelling forced by the strong equatorward winds. During each period of wind relaxation (not shown), the LC rapidly dominates the surface signal by overflowing the area with warm tropical waters (less than 12 h after the wind relaxation).

3.2. Regional Scale Water Mass Analysis

[20] The observed water mass distribution in autumn 2010 is quite typical to the region as described in detail by *Woo and Pattiaratchi* [2008] in the austral summer. Overall, five waters masses were sampled, including the lower salinity Tropical Surface Water (TSW), the higher salinity South Indian Central Waters (SICW), the higher oxygen Sub-Antarctic Mode Water (SAMW), the deep lower salinity Antarctic Intermediate Water (AAIW), and the deep lower oxygen North West Indian Intermediate Water (NWIIW) (Figure 3). The oxygen (Figure 3a) and nitrate concentrations (Figure 3b) as derived from the oxygen and ISUS high-resolution sensors are added on the potential temperature (T)/absolute salinity (S) diagrams. Their vertical partition is quite similar to the one presented by *Woo and Pattiaratchi* [2008] with the TSW from the surface till 100–150 m, above the SICW (from 150 to 350 m), lying on the SAMW (from 350 to 500 m), followed by the AAIW from 500 till about 750 m, and finally the NWIIW from 750 till 1000 m. Note that, at these latitudes, the SAMW and AAIW are slightly thicker (150 and 250 m, respectively) than the data reported by *Woo and Pattiaratchi* [2008] (100 and 180 m, respectively).

[21] In our data set, the TSW were slightly warmer (>25°C) and more saline (34.8–35.2) than during the austral summer period [*Woo and Pattiaratchi*, 2008]. The nutrient content of these waters is usually low (nitrate ≤ 1 μmol/L), associated with relatively high oxygen concentrations (>190 mol/L) in the euphotic layer (depth < 150 m). There are a few exceptions with relatively high nitrate concentrations (4–8 μmol/L) and low oxygen concentrations (<160 μmol/L) observed in relatively light waters ($\sigma < 23.9$). Although characterized by a T/S signature matching the TSW, these abnormally elevated nitrate concentrations suggest they originate from the LDOHN [*Woo and Pattiaratchi*, 2008; *Thompson et al*., 2011], being brought to the surface by diapycnal mixing and/or vertical movements such as upwelling. The SICW are characterized by very variable but slightly higher nitrate concentrations (1–6 μmol/L) than the TSW and lower than the LDOHN. Similarly, there is an inverse relationship between oxygen and nitrate concentrations in some of these waters, indicating a possible mixing between the LDOHN and the SICW.

[22] Indeed, the LDOHN consists in a local nitrate maximum (between 6 and 13 μmol/L) associated with particularly low dissolved oxygen content (below 160 μmol/L), situated on average between ~110 and 230 m, which correspond in this region to a density range of about $23.6 < \sigma < 26.2$. Its T/S signature is very variable and spreads along the interface between the TSW and the SICW (Figures 3a and 3b), suggesting an in situ biogeochemical process happening at the interface between these interleaving water masses. There are also some data points situated within the "elbow" constituted by the SICW (i.e., lower salinity), characterized by very high nitrate content for these depths (>10 μmol/L). These data are somehow unique since they have a T/S signature close to the deeper SAMW, indicating a possible mixing between SAMW/SICW and then later with TSW.

[23] The SAMW are formed by deep winter convection [*Woo and Pattiaratchi*, 2008] and are thus characterized by high concentrations of oxygen (> 220 μmol/L) and nitrate (8–16 μmol/L). The LU has been shown to be mainly composed of SAMW, although it may contain some SICW in the upper layers [*Woo and Pattiaratchi*, 2008]. In our data set, the LU was observed along sections 2, 3, 4, 6, and 7 at relatively shallow depths (~150–200 m) off the Ningaloo Peninsula during the cruise (see also Figure 9c), which is consistent with thicker SAMW as compared to the summer period.

[24] Finally, the AAIW and NWIIW have quite stable chemical characteristics over small spatiotemporal scale and thus match well the description made by *Woo and Pattiaratchi* [2008].

3.3. Offshore Interaction Between the MLD Deepening and the LDOHN Layer

[25] The 21°S cross-shore section (section 1) was sampled under relatively calm conditions, and the density contours indicated a downward slope toward the coast (Figure 4a), with southward velocity from 0.2 to 0.4 m/s in the top 120 m (not shown). The downwelling signal was observed consistently along sections 1, 2, and 3 (not shown), whereas the wind varied from downwelling to upwelling-favorable forcing when sampling these sections. Although the local downwelling-favorable winds may contribute to the observed downwelling signal, these observations strongly suggest that it is essentially due to a strong downwelling-favorable LC [*Woo and Pattiaratchi*, 2008; *Pattiaratchi and Woo*, 2009].

[26] The chlorophyll *a* distribution clearly shows a well-mixed local maximum inshore (~0.33 to 1 mg/m^3), while the rest of the section off the shelf break is characterized by a deep chlorophyll maximum (DCM) situated roughly between 50 and 100 m with concentrations of 0.1–1 mg/m^3. The coastal maximum is characterized by a relatively high contribution (8–12%) of cells larger than 5 μm in the whole water column (Figure 4a), significant in these oligotrophic waters [*Hanson et al*., 2005]. The size distribution in the offshore waters shows a different pattern: large phytoplankton (> 5 μm) is very sparse in the surface waters and in the DCM (0%–4%), but it increases just below the DCM (5%–10%), although at low total concentrations (0.05 mg/m^3). The offshore surface waters are depleted in chlorophyll *a* (<0.1 mg/m^3), except at some particular location that seems to be characterized by a local deflection of the isopycnals.

[27] To further investigate this phenomenon, the MLD was calculated using three different criteria based on temperature (T), salinity (S), and buoyancy frequency gradients, respectively. Following *Lourey et al*. [2006], the MLD is defined as the minimum depth at which $|T - T_{10m}| > 0.4$ or $|S - S_{10m}| > 0.03$. We also recorded at each CTD profile the minimum depth where the buoyancy frequency reaches a threshold of 2.10^{-4} rad^2/s^2. A good agreement (regression

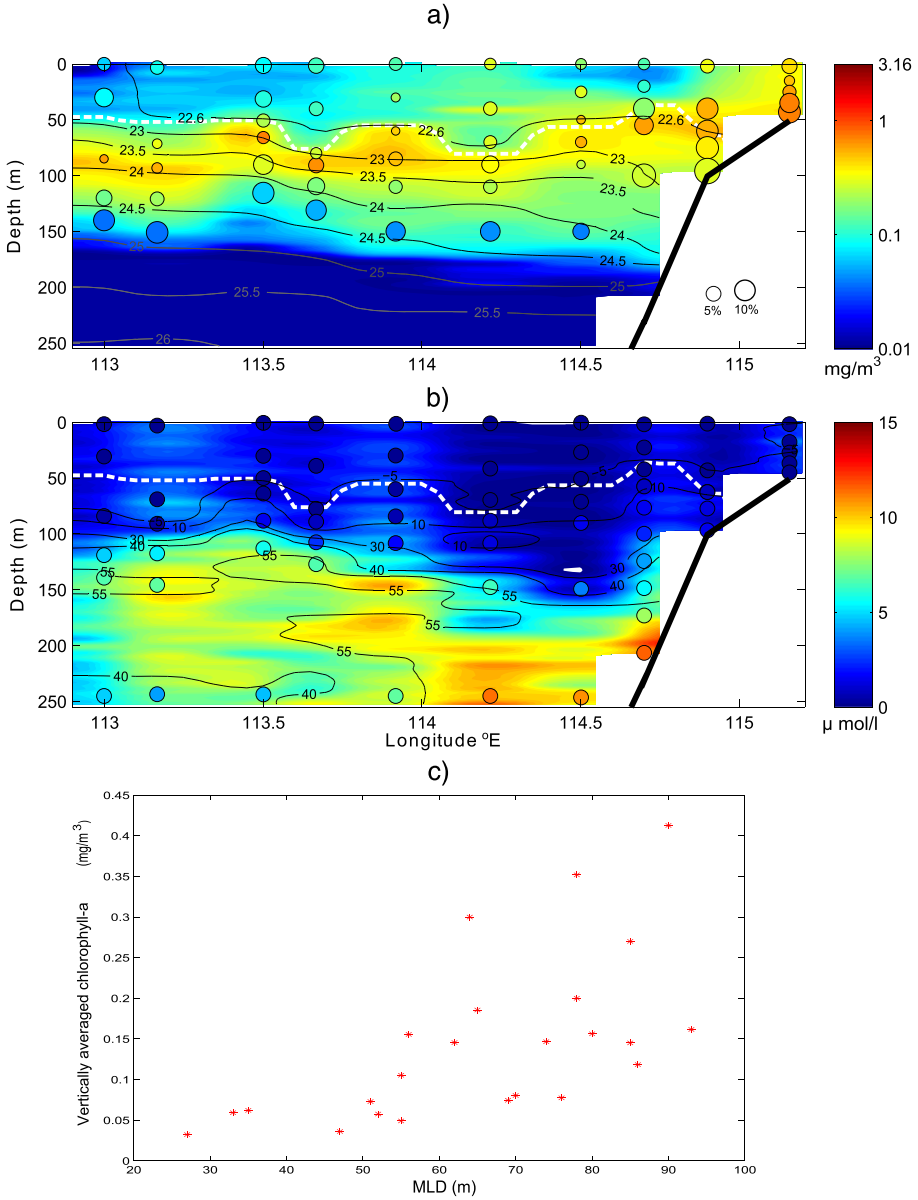

Figure 4. Offshore dynamics. Longitude versus depth section of CTD sensors and water sample measurements along transect 1 at 21°S. (a) Chlorophyll *a* ($\log_{10}$) from the fluorometer (calibrated versus water samples, $R^2 = 0.6$), with black/gray contours representing the density field. The filled circle represent the water samples measurements, color is chlorophyll *a* concentration, while the size of the circle is proportional to the percentage of large phytoplankton cells (larger than 5 μm). (b) Nitrate concentrations (μmol/L, from the ISUS), with black contours representing the AOU (μmol/L). The filled circles represent the water sample measurements of nitrate in μmol/L. On both panels, the thick black line is the observed topography, and the white dotted line is the MLD calculated from temperature gradients. (c) Vertically averaged chlorophyll *a* (mg/m^3) versus MLD (m) per CTD station in the LC (more than 50 km off the coast).

factor ~ 1, $R^2 \geq 0.85$) is found between the three different methods to compute the MLD. The inshore stations (<50 km from the coast) were excluded from the analysis due to the particular chlorophyll dynamics there. The MLD shows high temporal and spatial variability and oscillates between 20 and 100 m during our cruise. *Rousseaux et al.*'s [2012] hypothesis about the MLD deepening favoring the autumn bloom was tested by averaging converted chlorophyll *a* (from the fluorometer) from the surface to the MLD at each offshore station. Although some dispersion exists, there is a clear positive relationship between the depth of the MLD and the vertically averaged chlorophyll *a* (Figure 4c).

[28] Examining the nitrate profile (Figure 4b), it is difficult to associate a deep MLD with enhanced nutrient concentrations since the nutrient injection at the surface is likely to be rapidly followed by intense phytoplankton uptake. However, considering sections of nitrate, AOU, and chlorophyll *a* together, their relationship becomes clearer. In the surface waters (0–100 m), high chlorophyll concentrations are generally characterized by near-depleted waters (nitrate

1 µmol/L) and small or even negative AOU (<10 µmol/L, production of oxygen by photosynthesis). In the subsurface waters, just below the DCM with moderated chlorophyll *a* concentration, there is a sharp gradient in both nitrate and oxygen. Within 10–20 m, nitrate increases rapidly from ~2 to 8–12 µmol/L, while AOU goes from ~10 up to 40–60 µmol/L. Finer-scale coupled structures are observed at the subsurface (depth > 100 m, at the interface between the TSW and SICW): there is a good coherence between local maxima of nitrate and AOU (Figure 4b). To better quantify this relationship, we computed spatial correlations of the vertical profiles of AOU versus nitrate (1 m binned data, smoothed over three indices) within the range of density $23.6 < \sigma < 26.2$ (corresponding in average to depths of ~110–230 m), as identified in section 3.2. Among all the surveyed stations, we investigate this relationship within the ~40 stations off the shelf. Spatial correlations of subsurface AOU/nitrate range from 0.5 to 0.98, averaging up to ~0.8 (all statistically significant at the 99% confidence levels). This tight coupling of small-scale variations of AOU/nitrate is observed over the entire surveyed region (Figure 5). Although there is an apparent decoupling at very small vertical scales (<3 m), every local maximum of nitrate at the subsurface is characterized by a simultaneous increase of AOU. It symbolizes thin "layers" (from a few meters to ~50 m thick) of intense remineralization of nitrate through consumption of oxygen, in line with our previous observations based on the water mass analysis. This relationship is explored in more details by Waite et al. [2013].

3.4. Evidence of Submesoscale Eddies

[29] The area south of Point Cloates was sampled twice during the cruise using the Nacelle towed body, thus providing high-resolution coverage of the top 200 m of the water column. On both occasions, submesoscale eddy-like structures were observed to impact the local stratification (Figures 6 and 7). The first submesoscale eddy A is cyclonic of about 21 km in diameter and was observed on 17 May, during the short period of wind reversal following 4 days of strong northward winds. This vortex-like structure is very intense as indicated by the strong alternating velocities (±0.4 m/s) and extends till 180 m. It resulted in the vertical uplift of the isopycnals in the core of the eddy. In particular (Figures 6a and 6c), the isopycnal $\sigma = 23.25$ is uplifted from 60 m and outcrops at the surface, corresponding to a vertical movement of more than 60 m, while a deeper isopycnal ($\sigma = 23.75$) undergoes a 20 m uplift (from 130 to 110 m deep). The same area was sampled again on 22 May (after the wind reversal), and a pair of cyclonic eddies (B and C) was observed (~20 km diameters). Although these structures seem less intense than the previous eddy according to their velocity signatures (extending to 160 and 100 m, respectively; Figure 7a), they are associated with subsequent uplift of the isopycnal with a vertical displacement of the isopycnal $\sigma = 23.5$ of about 30 m in the center of both eddies (Figure 7b).

[30] To better understand the physical structure of these submesoscale eddies, we investigate the ratio of the relative vorticity ζ and the Coriolis parameter f. As horizontal velocities are available only along ADCP transects thought to cross the eddy center, we approximate the relative vorticity ($\zeta = \frac{\partial v}{\partial x} - \frac{\partial u}{\partial y}$) to a single component (i.e., $\frac{\partial v}{\partial x}$ for transect (i) being almost zonal and $-\frac{\partial u}{\partial y}$ for transect (ii) being almost meridional). Following *Feng et al.* [2007], the relative vorticity ζ is averaged within each eddy diameter and is then compared to the Coriolis parameter $f = -2\Omega \sin(\text{latitude}) \approx 5 * 10^{-5}$ s^{-1} at 22°S–23°S. For the cyclonic eddy A, centered at 113.425°E along transect (i), we found

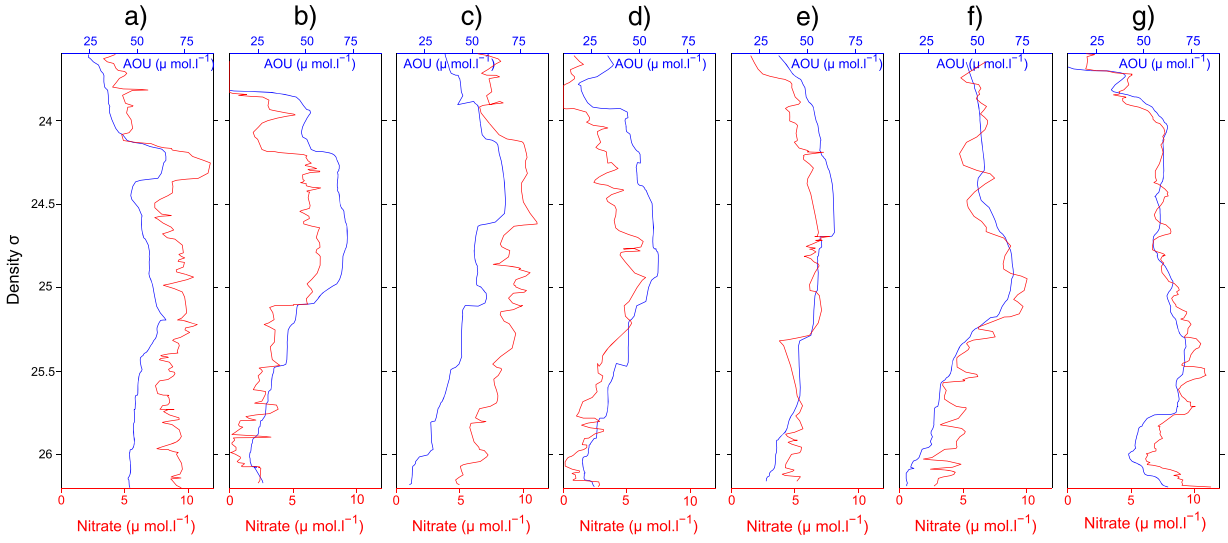

Figure 5. Subsurface biogeochemistry. Subsurface vertical profiles (1 m binned) of AOU (µmol l^{-1}) and nitrate (µmol l^{-1}) against density ($23.6 < \sigma < 26.2$) selected along each section. (a) Station 8/section 1, (b) station 19/section 2, (c) station 27/section 3, (d) station 32/section 4, (e) station 39/section 5, (f) station 43/section 6, and (g) station 50/section 7. Correlation coefficients between these variable are 0.87, 0.9, 0.86, 0.82, 0.73, 0.86, and 0.88 (all significant to the 99% confidence level) for Figures 5a, 5b, 5c, 5d, 5e, 5f, and 5g, respectively.

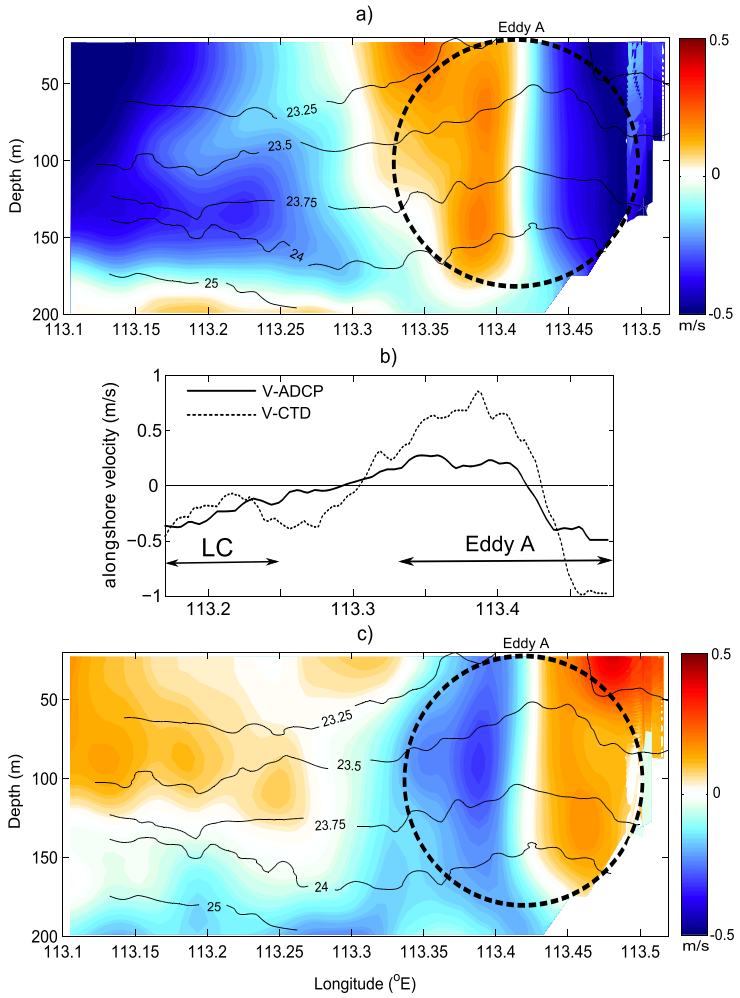

Figure 6. Submesoscale eddy along transect (i). (a) Alongshore and (c) cross-shore currents from the vessel ADCP along. Black contours represent isopycnals derived from the nacelle towed body. (b) Alongshore surface velocities derived from the geostrophic calculation referenced to 180 m ADCP data (dotted line) versus the measured ADCP surface velocities (black line). In Figures 6a and 6c, red color indicates northward (onshore) current on the alongshore (cross-shore) profile and the black dotted ellipse indicates the submesoscale eddy A.

$\zeta = -1*10^{-4}$ s^{-1}, resulting in a ratio of $\left|\frac{\zeta}{f}\right| \approx 2$. The elevated relative vorticity within eddy A suggests it is highly nonlinear. For the cyclonic eddy B (C, respectively), centered at −22.85°S (−22.6°S, respectively) along transect (ii), we found $\zeta = -1.5*10^{-5}$ s^{-1} ($\zeta = -1.3*10^{-5}$ s^{-1}, respectively) resulting in a ratio of $\left|\frac{\zeta}{f}\right| \approx 0.27$ ($\left|\frac{\zeta}{f}\right| \approx 0.24$, respectively). It suggests that about 20%–30% of the total velocities are due to the centrifugal terms [*Feng et al.*, 2007]. In addition, the geostrophic velocities computed from the CTD profiles (towed nacelle) are compared to the shear of the ADCP velocities (Figure 6b). More specifically, we use an upward integration of the thermal wind law from a reference level of no motion to derive the "CTD" geostrophic velocity with reference to ADCP velocities at these levels (180 m for transect (i) and 160 m for transect (ii), as the shallow depths of the continental shelf restricted the vertical extension of the data). The "ADCP" and "CTD" velocities are in quite good agreement from ~113.1°E to 113.3°E, i.e., within the LC, which thus seems to be in "geostrophic balance." Within eddy A (113.3°E–113.5°E), the "CTD" velocities are largely higher than the "ADCP" ones, consistent with the strong nonlinearity of eddy A (and to a lesser extend in eddies B and C, not shown). These analyses are in good agreement with the results of *Feng et al.* [2007] and with the ratios $\frac{\zeta}{f}$ previously calculated. While eddy A seems to have been sampled through its center, the moderate nonlinearity found for the submesoscale eddies B and C is possibly related to a partial sampling through their flanks.

[31] Unfortunately, there is no reliable biological data in these small-scale structures due to the disfunctioning of the fluorometer, and no water sampling was carried out. Nevertheless, it is evident that such vertical movements up to 60 m will bring subsequent nutrients to the euphotic layer and would thus stimulate phytoplankton production locally.

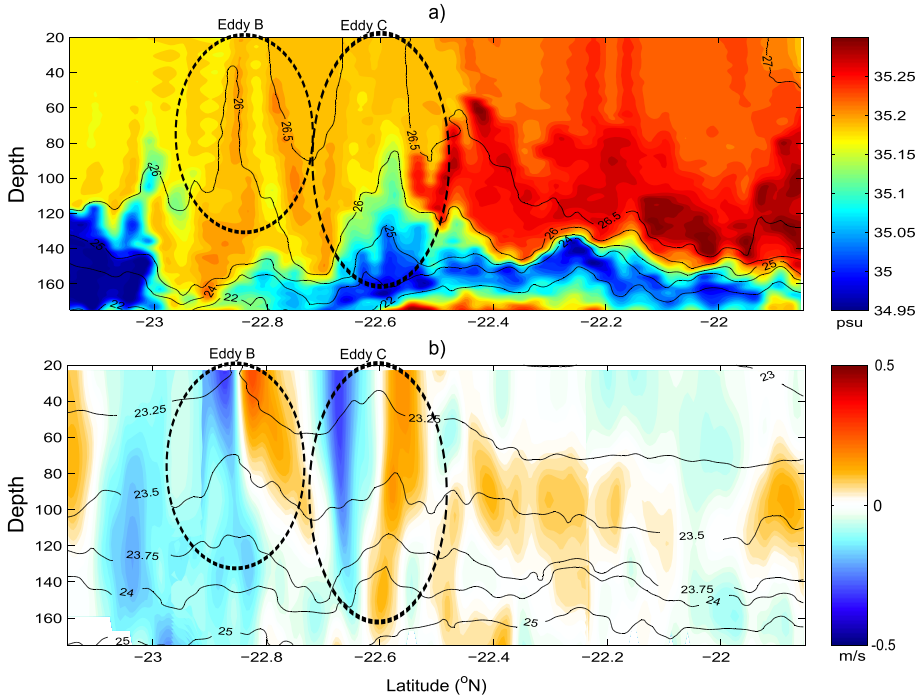

Figure 7. Submesoscale eddy along transect (ii). (a) Profiles of salinity with temperature contoured and (b) corresponding cross-shore currents with density contoured. Red color indicates onshore current on the cross-shore profile. Black dotted ellipses indicate the submesoscale eddies B and C.

3.5. Evidence of Coastal Upwelling in Autumn 2010

[32] Upwelling-favorable wind occurred from 12 to 16 May and from 18 to 25 May (Figure 2b). The appearance of relatively cold waters inshore was visible on the SST snapshots (Figures 2a2 and 3) close to the coast, while the warm LC waters were pushed offshore, as mentioned in *Pattiaratchi and Woo* [2009]. In situ data reveals a clear surface response of the successive wind-driven upwelling events (Figure 8a). As compared to the water flowing offshore ($T \sim 27.5°C$; $\sigma \sim 22.8$), relatively colder ($T < 26°C$) and denser ($\sigma > 22.9$) waters are found at the coast from the most southern section (Figure 8a1). These upwelled waters are significantly richer in phytoplankton with up to 0.5 mg/m^3 of vertically averaged chlorophyll *a* in the top 50 m, whereas mean concentrations are between 0.1 and 0.01 mg/m^3 offshore, omitting the DCM (Figure 8a2).

[33] These events were also characterized by a reversal of the current inshore and the presence of the ephemeral NC. Selected ADCP sections and drifter trajectories demonstrated this sporadic current reversal (see Figure 8b). The blue arrows represent the integrated currents between 20 and 50 m measured by the vessel-mounted ADCP on 22–23 May. They show a strong southward current off the Ningaloo Peninsula and offshore (LC), while the northward NC is flowing continuously along the 200 m isobath (along the ship track, Figure 8b1). All the drifters were advected southward in the LC for about 120 km over 8 days, corresponding to a mean velocity of ~0.4 m/s. The two inshore trajectories were approaching the shelf and then suddenly reversed northward in the NC, on 20 and 22 May, respectively, while being characterized by lower SST (Figure 8b2). The change of the upper circulation is also evidenced by the westward shift of the surface currents derived from satellite (Figure 2a3). Once in the NC, the drifters reached northward velocities of about 0.2 m/s up to a maximum of 0.5 m/s during the peak of the second wind event (24 May).

[34] Section 6 was selected to investigate the detailed oceanic response under a sporadic wind-driven upwelling event and associated coastal counter current. The ADCP section reveals a strong NC (up to 0.45 m/s, consistent with the drifter data) located at the shelf break (Figure 9c). Although the NC is usually confined to the very nearshore area [*Pattiaratchi and Woo*, 2009], as observed along sections 3, 4, 5, and 7 (not shown), it can also meander offshore with some excursions along the shelf break (e.g., section 6). The isopycnals in the first 150 m ($\sigma < 23.25$) are subsequently uplifted toward the coast, whereas they remain flat in deeper waters (Figure 9a). This seems to indicate the origin of the upwelled waters is between 100 and 150 m, coinciding with the top of the LDOHN layer. Comparing the offshore (113.3°E) and the inshore casts (113.4°E and 113.5°E), it is evident that there is "erosion" of the LDOHN's upper layers close to the shelf break. The localized upwelling brings thus new and regenerated nutrient (3–7 µmol/L) onto the shelf to the surface/coast, triggering a strong biological response characterized by high chlorophyll *a* (> 0.5 mg/m^3) and local minima of AOU (<5 µmol/L and even negative values in the NC). Previous studies indicated that the NC is composed of water sourced from upwelling of relatively shallow (~100 m) enriched water from the base of the LC [*Hanson et al.*, 2005; *Woo et al.*, 2006a; *Woo and Pattiaratchi*, 2008], whereas in our observations, the source of the upwelling seems deeper (~150 m) probably due to a

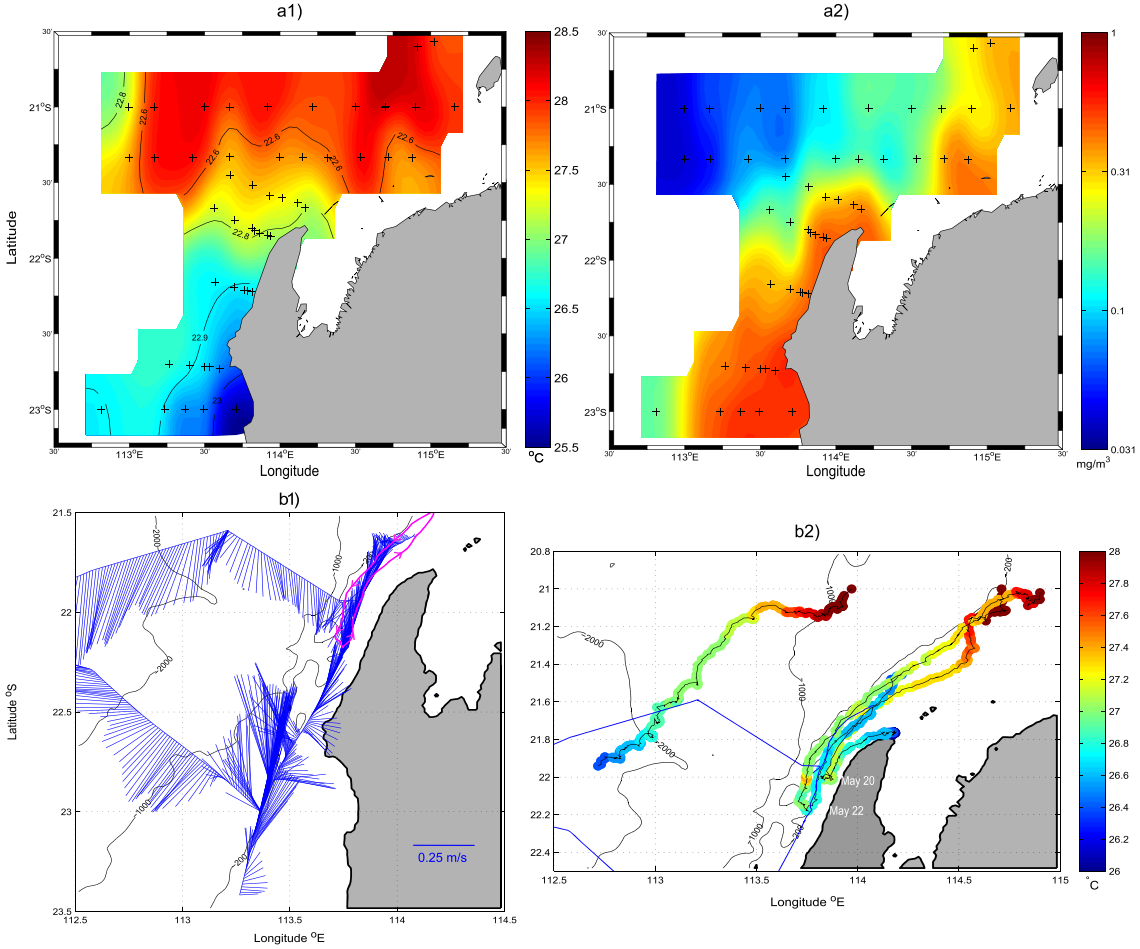

Figure 8. (a) Surface (5–50 m) averaged CTD over the whole area: (a1) temperature with density contoured and (a2) vertically averaged chlorophyll *a* (mg/m^3, from the fluorometer calibrated with water samples). Black crosses represent the CTD stations. (b1) Surface ADCP currents (along the ship track, integrated between 20 and 50 m) in blue measured on 22–23 May. The magenta line represents a drifter trajectory. (b2) Drifter trajectories with SST color; blue lines represent the ship track. The black thin lines are isobaths.

thicker MLD and/or stronger upwelling. Note again the tight coupling between AOU and nitrate at small scales, with a coincidence of local maxima of both variables (see, for instance, the blob of AOU ~ 15 µmol/L at the shelf break, associated with nitrate concentrations of ~3–4 µmol/L on Figure 9b).

[35] A clear distinction between the water masses constituting the NC and LC is evidenced by their different biophysical properties using the three most southern sections in the top 120 m (Figure 10). The LC is characterized by relatively homogeneous waters (low salinity) with poor chlorophyll *a* content and high AOU. The NC is composed of dense waters (colder and more saline) characterized by small or even negative AOU, a sign of high biological productivity. As a result, high phytoplankton biomass (chlorophyll $a > 0.5$ mg/m^3) is found in the whole water column of the NC whereas the LC waters are relatively poor and vertically heterogeneous. Although localized in space and occurring in autumn, a period thought to be not favorable for upwelling, this event was characterized by a clearly documented biological response.

4. Discussion

4.1. Large-Scale Context and Hydrography

[36] The field survey carried out during the austral autumn provides a high-resolution picture of the north-west region where the LC consolidates as a well-defined surface boundary current. A general water mass analysis revealed the presence of the typical water masses of the Leeuwin system, namely the TSW, the SICW, the SAMW, the AAIW, and the NWIIW. Their characteristics were quite similar to those presented by *Woo and Pattiaratchi* [2008], although a few differences remain. In particular, the TSW, derived from the Australasian Mediterranean Waters and formed in the surface Pacific Ocean during its transit via the Indonesian Archipelago [*Woo and Pattiaratchi*, 2008], was warmer and more saline than during the austral summer. First, it might be related to the seasonal variability of the source waters of the LC, being characterized by a stronger southward transport during this season and thus bringing more tropical waters from the Indonesian Throughflow [*Feng et al.*, 2008; *Weller et al.*, 2011]. It is consistent

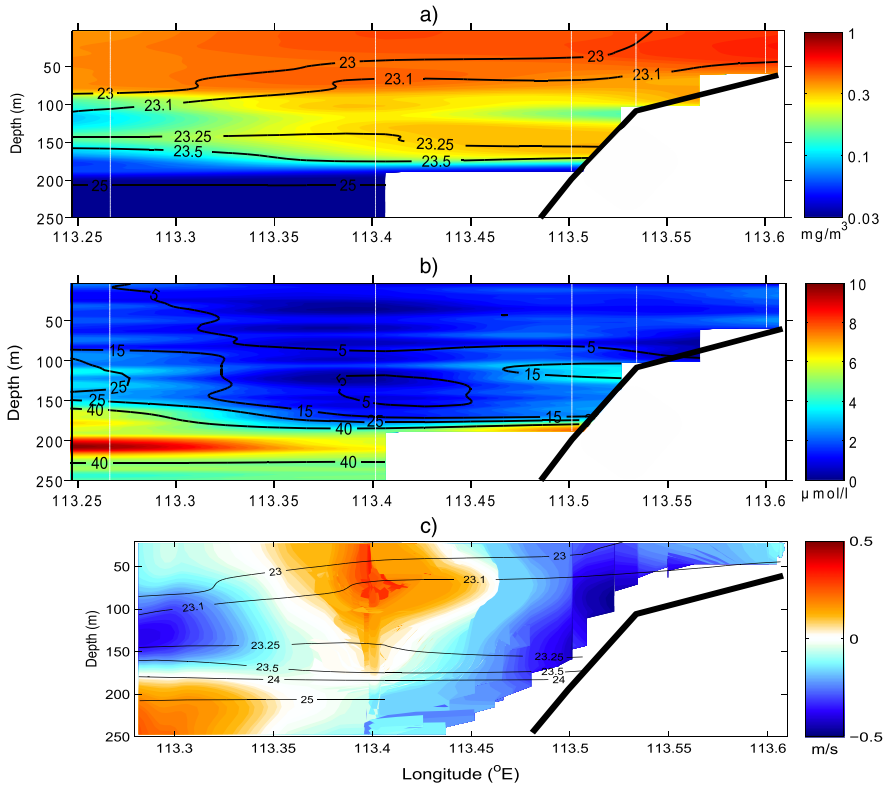

Figure 9. Longitude versus depth section 6 at 22.75°S: (a) is chlorophyll *a* coloured (mg/m^3) with contours of density superimposed; (b) represents the Nitrate concentrations (ISUS calibrated) with the AOU field contoured. (c) Alongshore current (m/s) from the vessel ADCP (red color indicates northward flow). Note the core of the NC (northward velocities > 0.3 m/s) at the surface, associated with a northward slope current (shallow LU), while most of the water is flowing southward (LC).

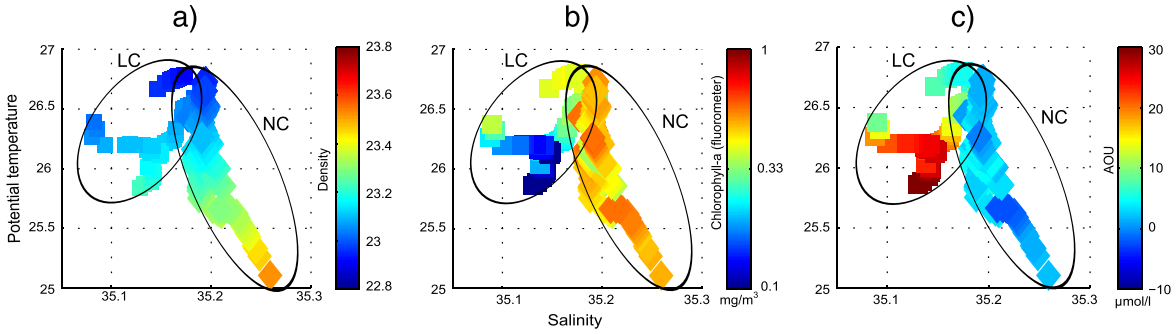

Figure 10. Temperature/salinity diagrams for the surface waters (top, 120 m) using the three most southern sections, colouring represents respectively (a) the density (σ), (b) the chlorophyll *a* (mg/m^3, $\log_{10}$), and (c) AOU (µmol/L).

with the analysis of *Domingues et al*. [2007], who found two pathways contributing to the TSW in the LC, originating from both the Indonesian Throughflow and a more northwestern source named the Gyral Current. Second, there is important interannual variability in the LC transport associated with the El Niño Southern Oscillation [*Feng et al*., 2008]. During La Niña years, the LC transport is maximal, whereas it is moderated during El Niño events. There was a sharp transition between a positive ENSO signal early 2010 (El Niño) to a strong negative signal (La Niña) at the end of the year, while a neutral situation prevailed in May 2010, so that the direct influence from interannual climate variation on the LC transport during autumn 2010 may not be significant. The Indonesian Throughflow and the Leeuwin Current were slightly weaker during the 2009/2010 El Niño event, so that the TSW may have experienced stronger evaporation and less freshwater fluxes from the Western Pacific and the Indonesian archipelago, thus resulting in saline surface condition.

[37] The SAMW layer was also slightly thicker than the observations by *Woo and Pattiaratchi* [2008], possibly due to the interannual variability of the winter convection south of Australia. This could also be related to the relatively strong and shallow LU observed throughout the region during the cruise, as simulated farther south by *Meuleners et al*. [2007]. Indeed, the LU flow can be associated with an offshore divergence and uplift along the slope, as indicated by some preliminary analysis based on a climatological data set (not shown) that indicated subsurface (~250 m) offshore geostrophic flow at 20°S–24°S during autumn mainly.

4.2. Subsurface Biogeochemistry Off Ningaloo

[38] The high-resolution data provided by the nitrate sensor provide unprecedented description of the LDOHN layer. It was observed almost over all the surveyed area except at the most northern transect, which seems to support the hypothesis of local (in situ) remineralization rather than its advection as speculated by *Thompson et al*. [2011]. Our observations also suggest that the LDOHN is not a specific water mass characterized by predefined physical properties as they vary substantially, as a result of the vertical mixing between water masses. It appears rather due to intense biogeochemical processes occurring at the interface of two or more water masses, namely the TSW, SICW, and even SAMW. In addition, the observed small-scale coupled structures of AOU/nitrate resulting in those fine "layers" suggest a tight coupling between biogeochemical and physical dynamics. In situ remineralization is likely to be the mechanism responsible for the observed subsurface nitrate off Ningaloo, while the surface depleted waters are characterized by intense phytoplankton uptake and other biogeochemical processes. Further details about the biogeochemistry in this region can be found in *Waite et al*. [2013].

[39] Based on the buoyancy profiles, some sections were characterized by two strong local gradients of density, the classical one at the base of the MLD (~60 - 100 m) while another one was situated between 180 and 250 m, constituting the boundary between SICW and TSW. Local maxima of nitrate (up to 12 μmol/L) and AOU (up to 55 μmol/L) were sometimes observed in between these physical boundaries, proof of intense in situ microbial respiration (not shown). These observations seem to further support an in situ process of remineralization occurring along sharp interfaces such as the ones between TSW and SICW and between SICW and SAMW, favored under "physical isolation." We also speculate that the SAMW, particularly thick at this time of the year, associated with an abnormally shallow and strong LU (see also Figure 9c), could help provide the oxygen needed for oxic remineralization processes (LDOHN) by subsurface geostrophic divergence and diapycnal mixing.

[40] In addition, cross-shelf dynamics might possibly promote the subsurface microbial respiration. Intense dense water formation from the inner shelf (enriched in organic matter) occurs during the autumn/winter period [*Pattiaratchi et al*., 2011] and might subduct under the TSW but sit on top of the next strongest physical gradient (in general the SICW), promoting the LDOHN.

[41] Overall, an inverse multiparametric model [e.g., *Paulmier et al*., 2006] can allow separating the contribution of physical mixing and of in situ biogeochemical processes. In addition, due to the numerous small-scale structures observed, high-resolution biophysical coupled modeling will provide new insights about its functioning.

4.3. Offshore Biophysical Coupling

[42] We have tested the mechanism proposed by *Rousseaux et al*. [2012] and found a positive correlation between vertically averaged chlorophyll *a* and the depth of the MLD in the LC waters. However, to fully test *Rousseaux et al*.'s [2012] hypothesis of an MLD deepening due to increasing surface air-sea heat fluxes in the LC, a more comprehensive comparison with the condition outside of the LC waters would be needed. The exclusion of the coastal stations in this analysis suggests there could be a different mechanism for planktonic biomass enhancement inshore. In summary, the chlorophyll *a* distribution in autumn reveals two different regimes. On one hand, the offshore productivity and its DCM appear to be driven by the deepening of the MLD due to large-scale (heat transfer) [*Rousseaux et al*., 2012] and local forcing (wind blowing against the LC) that will erode subsequently the relatively shallow source of nutrients (LDOHN). Note that the strong shear between the southward LC and the underlying water (usually flowing northward because of the presence of the LU) may also enhance vertical mixing at the subsurface. On the other hand, the surface primary production of the inshore domain (to the shelf break) seems influenced by localized nutrient enrichment processes as discussed in the following.

4.4. "Topographically Trapped" Submesoscale Eddies

[43] Twice during the study, we observed submesoscale eddies creating subsequent uplifting in their core in the vicinity of Point Cloates. Complex recirculating flows are common in this area [*Taylor and Pearce*, 1999; *Woo et al*., 2006a] and have been associated with the interactions between the southward meandering LC, the northward flowing NC, and the coastal promontory of Point Cloates. *Woo et al*. [2006b] studied the dynamics of this recirculation pattern using satellite imagery and numerical modeling, and they indicated that a combination of southerly winds and the local topography is responsible for the anticlockwise recirculation. Here we observed a cyclonic eddy first and a pair of cyclonic submesoscale eddies 5 days later. These observations demonstrate that the recirculation pattern seems to be a persistent feature of this area, although being more complex than previously thought. *Woo et al*. [2006b] also showed that stronger southerly winds generated a higher volume transport in the NC, but that the recirculation feature was inversely correlated with the wind speed. Our local observations strengthen their model-based conclusions since the eddy structures were observed under weak or even reversed wind conditions, while the northward flow of the NC was still present.

[44] Contrarily to what was found by *Feng et al*. [2007] studying open-ocean mesoscale eddies, the isothermal doming at the center of the cyclonic submesoscale eddies did reach the surface euphotic zone, so that there was active upwelling at the core of eddy A (and to a lesser extent of eddies B and C). These submesoscale eddies associated to

a meandering LC interacting with the shelf topography were characterized by an efficient upwelling in their core due to their highly nonlinear nature revealed by our analysis.

[45] Other regions along the WA coastline have also been identified as preferential location for submesoscale and mesoscale eddy formation such as south of the Abrolhos Island [*Feng et al*., 2005] and the Perth Canyon [*Rennie et al*., 2007], in relation to complex topographic features. Although the physical mechanisms to form and maintain these persistent submesoscale eddy-like structures remain unclear, we hypothesized that their repetitive occurrence might have important biological consequences in providing both the required retention for coral/fish spawning and a subsequent nutritional source by promoting planktonic production locally through the uplift of nutrients [*Bakun*, 1996; *Taylor and Pearce*, 1999].

4.5. Dynamics of the Coastal Countercurrent

[46] Successive upwelling-favorable wind events prevailed during our campaign and resulted in a localized but significant upwelling event, associated with the occurrence of the coastal countercurrent, the NC.

[47] While we did not capture its full dynamics, an analysis of the ADCP and drifter data together indicated that the NC initiated around 13 May, restricted to the very inner shelf (from 5 to 10 km off the coast), and it then extended farther offshore while its intensity increased during the second wind event from 18 May onward. Our localized observations suggest that the NC requires alongshore northward winds (~10 m/s) to form, with successive wind events possibly cumulating their effects by both strengthening and extending it offshore. This is consistent with the analysis based on a regional modeling study by *Woo et al*. [2006b], who showed that both the NC transport and its offshore extension are positively correlated with the alongshore wind stress. It is also in agreement with a theoretical numerical study by *Rossi et al*. [2010], who demonstrated that strong transient alongshore winds can generate significant currents on the shelf to the shelf break. In particular, the equatorward alongshore wind stress generates a northward flow intensified in the upper layers near the coast and a barotropic current extending over the whole shelf, which rapidly weakens over the continental margin as the total depth increases drastically, especially over the narrow shelf of the Ningaloo Peninsula region. This can explain why the correlation between alongshore wind stress and alongshore surface current is higher inshore (50 m isobath) than offshore (100 m) in the moored data presented by *Lowe et al*. [2012]. However, the inshore circulation established by the alongshore wind will be maintained even when the wind has stopped (geostrophic equilibrium attained) and only slowly dissipate, mainly by bottom friction. There is fast dissipation if strong opposite forces follow, such as opposing winds or currents. Because the LC (forced by a persistent pressure gradient) will rapidly overflow the outer shelf after any upwelling-favorable wind event, the countercoastal currents are often confined to the very inshore area over the WA coast. In the south-west region, *Gersbach et al*. [1999] found this transitional isobath to oscillate between 50 m under a weak alongshore wind stress to 150 m for a maximal wind stress, restraining inshore (less than 15 km) the coastal countercurrent for the narrow shelves such as the Ningaloo region. The opposing role of the wind and pressure gradient seem to be controlling the alongshore flows, as suggested by the observations in the Geelvink Channel of *Cresswell et al*. [1989]. In addition, *Lowe et al*. [2012] recently observed that the inner shelf currents off Ningaloo are only weakly influenced by the LC and that there is no consistent summer time wind-driven NC.

4.6. Biological Impacts of the Coastal Upwelling

[48] Contrary to prior belief, we have documented a localized upwelling event off Ningaloo Peninsula during austral autumn. Based on our field data, we estimate that the upwelled waters are originating between 100 and 150 m, coinciding with the top of the LDOHN layer (erosion of the subsurface nitrate maximum) and thus feeding the euphotic layer with subsequent nutrient concentrations. *Hanson et al*. [2005] and *Lowe et al*. [2012] observed the upwelling originating at about 100 m, whereas in our observations it seems slightly deeper (~100–150 m). Indeed, the upwelling process will source its waters beneath the LC and associated MLD, which in our case (autumn) was relatively deeper than previous studies (summer). These productive upwelled waters were mainly restricted over the continental shelf (because of the presence of the LC offshore) and thus probably continuously advected northward in the coastal countercurrent NC.

[49] *Furnas* [2007] argued that intermittent bursts of high productivity can occur in specific locations or circumstances over this coast, as it is expected in our observations due to the upwelling-favorable conditions. Indeed *Hanson et al*. [2005, 2007] reported levels of primary production of 3000–8000 mg C m^{-2} d^{-1} in the NC/upwelled waters (as compared to 200 mg C m^{-2} d^{-1} within the core of the LC). Although small phytoplankton such as cyanobacteria are thought to be dominant in these oligotrophic offshore waters (up to 80%), a significant increase of phytoplankton larger than 5 μm was observed at the coast and within the NC. This is in line with *Hanson et al*. [2007], who showed that, within countercurrents and shelf regions, diatoms were more abundant than in the LC. Among other, processes such as terrestrial inputs, sediment resuspension, and biogeochemical benthic-pelagic coupling might also influence the coastal productivity.

[50] A recent study by Rossi et al. (On the factors influencing the development of sporadic upwelling in the Leeuwin Current system, submitted to *Journal of Geophysical Research*, 2013) studied the occurrence of sporadic upwelling along the whole WA coast based on a composite upwelling index. At Ningaloo, the occurrence of sporadic upwelling and associated nutrient enrichment is favored during spring/summer but may also occur in autumn/winter. This might explain why the coastal communities are characterized by upwelling-ready species [*Hanson and McKinnon*, 2009], in contrast with the offshore microbial communities influenced by other processes described previously.

5. Conclusions

[51] Results from a multidisciplinary survey performed off Ningaloo region in austral autumn suggest that the hydrological characteristics seems relatively constant

throughout a seasonal cycle, although a few differences remain due to the seasonal and inter-annual variability of the LC transport and of its source waters. The LDOHN was consistently sampled across the whole region, but it was not characterized by a distinct *T*/*S* signature. Indeed, our observations suggest that local in situ remineralization from surface organic matter accumulating along sharp physical interfaces might be the most probable mechanism for its formation. It is hypothesized that diapycnal mixing of subsurface water masses (TSW, SICW, SAMW) and the surface intrusion of the LU may provide oxygenated waters needed for microbial processes.

[52] These subsurface-enriched waters in autumn are favoring surface biological activity through distinct mechanisms on and off the continental shelf. Enhanced levels of chlorophyll *a* offshore are associated with deeper MLD and the erosion of the LDOHN layer underneath. Inshore, highly nonlinear topographically trapped submesoscale eddies, localized upwelling events, and associated coastal countercurrents provide nutrient enrichments and retention pattern in the region. In response to the upwelling-favorable winds, we estimated the origin of upwelled waters to be between 100 and 150 m, slightly deeper than during the summer, thus uplifting new and remineralised nutrients.

[53] We have shown that there are complex interactions between synoptic (LC characteristics, "LDOHN" and MLD) and local (sporadic upwelling events and submesoscale eddies and meanders) processes, which have important consequences for the nutrient dynamics along the WA coastline.

[54] **Acknowledgments.** The authors acknowledge all the staff and crew from the *Southern Surveyor* and the Marine National Facilities. This research was supported under Australian Research Council's Discovery Project funding scheme (DP1093510) which also supports V.R. Microwave OI SST data are produced by Remote Sensing Systems and sponsored by National Oceanographic Partnership Program, the NASA Earth Science Physical Oceanography Program, and the NASA MEASURES DISCOVER Project. Data are available at www.remss.com. The authors would like to thank the anonymous reviewers for their valuable comments that have substantially improved this manuscript.

References

Bakun, A. (1996), Patterns in the Ocean: Oceanic Processes and Marine Population Dynamics (University of California Sea Grant, San Diego, CA, in cooperation with Centro de Investigaciones Biologicas de Noroeste, La Paz, Baja California Sur, Mexico).

Cresswell, G. R., and T. J. Golding (1980), Observations of a south flowing current in the southeastern Indian Ocean, *Deep Sea Res. Part A*, *27*, 449–466.

Cresswell, G. R., F. M. Boland, J. L. Peterson, and G. S. Wells (1989), Continental shelf currents near the Abrolhos Islands, Western Australia, *Aust. J. Mar. Freshwater Res.*, *40*, 113–128.

Domingues, C. M., M. E. Maltrud, S. E. Wijffels, J. A. Church, and M. Tomczak (2007), Simulated Lagrangian pathways between the Leeuwin Current system and the upper-ocean circulation of the southeast Indian Ocean, *Deep Sea Res. Part II*, *54*(8-10), 797–817.

Feng, M., G. Meyers, A. F. Pearce, and S. Wijffels (2003), Annual and interannual variations of the Leeuwin Current at 32°S, *J. Geophys. Res.*, *108*, 3355, doi:10.1029/2002JC001763.

Feng, M., S. Wijffels, S. Godfrey, and G. Meyers (2005), Do eddies play a role in the momentum balance of the Leeuwin Current?, *J. Phys. Oceanogr.*, *35*, 964–975.

Feng, M., L. J. Majewski, C. B. Fandry, and A. M. Waite (2007), Characteristics of two counter-rotating eddies in the Leeuwin Current system off the Western Australian coast, *Deep Sea Res. Part II*, *54*, 961–980.

Feng, M., A. Biastoch, C. Boning, N. Caputi, and G. Meyers (2008), Seasonal and interannual variations of upper ocean heat balance off the west coast of Australia, *J. Geophys. Res.*, *113*, C12025, doi:10.1029/2008JC004908.

Furnas, M. (2007), Intra-seasonal and inter-annual variations in phytoplankton biomass, primary production and bacterial production at North West Cape, Western Australia: links to the 1997–1998 El Niño event, *Cont. Shelf Res.*, *27*, 958–980.

Garcia, H. E., and L. I. Gordon (1992), Oxygen solubility in seawater: Better Fitting equations, *Limnol. Oceanogr.*, *37*(6), 1307–1312.

Gersbach, G. H., C. B. Pattiaratchi, G. N. Ivey, and G. R. Cresswell (1999), Upwelling on the south-west coast of Australia—source of the Capes current?, *Cont. Shelf Res.*, *19*, 363–400.

Hanson, C. E., and A. D. McKinnon (2009), Pelagic ecology of the Ningaloo region, Western Australia: Influence of the Leeuwin Current, *J. R. Soc. West. Aust.*, *92*, 129–137.

Hanson, C. E., C. B. Pattiaratchi, and A. M. Waite (2005), Sporadic upwelling on a downwelling coast: phytoplankton responses to spatially variable nutrient dynamics off the Gascoyne region of Western Australia, *Cont. Shelf Res.*, *25*, 1561–1582.

Hanson, C. E., A. M. Waite, P. A. Thompson, and C. B. Pattiaratchi (2007), Phytoplankton community structure and nitrogen nutrition in Leeuwin Current and coastal waters off the Gascoyne region of Western Australia, *Deep Sea Res. Part II*, *54*, 902–924.

Koslow, J. A., S. Pesant, M. Feng, A. Pearce, P. Fearns, T. Moore, R. Matear, and A. M. Waite (2008), The effect of the Leeuwin Current on phytoplankton biomass and production off South Western Australia, *J. Geophys. Res.*, *113*(19), C07050, doi:10.1029/2007JC004102.

Labasque, T., C. Chaumery, A. Aminot, and G. Kergoat (2004), Spectrophotometric Winkler determination of dissolved oxygen: re-examination of critical factors and reliability, *Mar. Chem.*, *88*(1-2), 53–60.

Lourey, M. J., J. R. Dunn, and J. Waring (2006), A mixed-layer nutrient climatology of Leeuwin Current and Western Australian shelf waters: Seasonal nutrient dynamics and biomass, *J. Mar. Syst.*, *59*, 25–51.

Lowe, R. J., G. N. Ivey, R. M. Brinkman, and N. L. Jones (2012), Seasonal circulation and temperature variability near the North West Cape of Australia, *J. Geophys. Res.*, *117*, C04010, doi:10.1029/2011JC007653.

Meuleners, M. J., C. B. Pattiaratchi, and G. N. Ivey (2007), Numerical modelling of the mean flow characteristics of the Leeuwin current system, *Deep Sea Res. Part II*, *54*, 837–858.

Moore, T. S., S. Thomas, R. J. Matear, J. Marra, and L. Clementson (2007), Phytoplankton variability off the Western Australian Coast: Mesoscale eddies and their role in cross-shelf exchange, *Deep Sea Res. Part II*, *54*, 943–960.

Parsons, T. R., Y. Maita, and C. M. Lalli (1984), *A manual of chemical and biological methods for seawater analysis*, Pergamon Press, New York.

Paterson, H. L., M. Feng, A. M. Waite, D. Gomis, L. E. Beckley, D. Holliday, and P. A. Thompson (2008), Physical and chemical signatures of a developing anticyclonic eddy in the Leeuwin Current, eastern Indian Ocean, *J. Geophys. Res.*, *113*, C07049.

Pattiaratchi, C., and M. Woo (2009), The mean state of the Leeuwin Current system between North West Cape and Cape Leeuwin, *J. R. Soc. West. Aust.*, *92*, 221–241.

Pattiaratchi, C., B. Hollings, M. Woo, and T. Welhena (2011), Dense shelf water formation along the south-west Australian inner shelf, *Geophys. Res. Lett.*, *38*, L10609, doi:10.1029/2011GL046816.

Paulmier, A., D. Ruiz-Pino, V. Garçon, and L. Farias (2006), Maintaining of the East South Pacific Oxygen Minimum Zone (OMZ) off Chile, *Geophys. Res. Lett.*, *33*, L20601, doi:10.1029/2006GL026801.

Rennie, S. J., C. Pattiaratchi, and R. D. McCauley (2007), Eddy formation through the interaction between the Leeuwin Current, Leeuwin Undercurrent and topography, *Deep Sea Res. Part II*, *54*, 818–836.

Ridgway, K. R., and Condie S. A. (2004), The 5500-km-long boundary flow off western and southern Australia, *J. Geophys. Res. 109*, doi:10.1029/2003JC001921.

Rossi, V., Y. Morel, and V. Garçon (2010), Effect of the wind on the shelf dynamics: formation of a secondary upwelling along the continental margin, *Ocean Modell.*, *31*(3-4), 51–79.

Rossi, V., M. Feng, C. Pattiaratchi, M. Roughan, and A. M. Waite (2013), On the factors influencing the development of sporadic upwelling in the Leeuwin Current system. Companion paper under revision in *J. Geophys. Res.*

Rousseaux, C. S. G., R. Lowe, M. Feng, A. M. Waite, and P. A. Thompson (2012), The role of the Leeuwin Current and mixed layer depth on the autumn phytoplankton bloom off Ningaloo Reef, Western Australia, *Cont. Shelf Res.*, *32*, 22–35.

Smith, R. L., A. Huyer, J. S. Godfrey, and J. A. Church (1991), The Leeuwin current off Western Australia, 1986-1987, *J. Phys. Oceanogr.*, *21*, 323–345.

Taylor, J. G., and A. F. Pearce (1999), Ningaloo Reef currents: Implications for coral spawn dispersal, zooplankton and whale shark abundance, *J. R. Soc. West. Aust.*, *82*, 57–65.

Thompson, P. A., K. Wild-Allen, M. Lourey, C. Rousseaux, A. M. Waite, M. Feng, and L. E. Beckley (2011), Nutrients in an oligotrophic boundary current: Evidence of a new role for the Leeuwin Current, *Prog. Oceanogr.*, *91*(4), 345–359.

Thompson, R. O. R. Y. (1987), Continental shelf-scale model of the Leeuwin current, *J. Mar. Res.*, *45*, 813–827.

Twomey, L. J., A. M. Waite, V. Pez, and C. B. Pattiaratchi (2007), Variability in nitrogen uptake and fixation in the oligotrophic waters off the south west coast of Australia, *Deep Sea Res. Part II*, *54*, 8–10.

Waite, A. M., S. C. Pesant, D. A. Griffin, P. A. Thompson, and C. M. Holl (2007), Oceanography, primary production and dissolved inorganic nitrogen uptake in two Leeuwin Current eddies, *Deep Sea Res. Part II*, *54*(8-10), 981–1002.

Waite, A. M., V. Rossi, M. Roughan, B. Tilbrook, J. Akl, P. A. Thompson, M. Feng, A. S. J. Wyatt, and E. J. Raes (2013), Formation and maintenance of high-nitrate, low pH layers in the Eastern Indian Ocean and the role of nitrogen fixation, *Biogeosciences Discuss.*, *10*, 3951–3976, doi:10.5194/bgd-10-3951-2013.

Weaver, A. J., and J. H. Middleton (1989), On the dynamics of the Leeuwin current, *J. Phys. Oceanogr.*, *19*, 626–648.

Weller, E., D. Holliday, M. Feng, L. Beckley, and P. A. Thompson (2011), A continental shelf scale examination of the Leeuwin Current off Western Australia during the austral autumn-winter, *Cont. Shelf Res.*, *31*, 1858–1868.

Woo, M., and C. B. Pattiaratchi (2008), Hydrography and waters masses off the Western Australian coast, *Deep Sea Res. Part I*, *55*, 1090–1104.

Woo, M., C. B. Pattiaratchi, and W. Schroeder (2006a), Summer surface circulation along the Gascoyne continental shelf, Western Australia, *Cont. Shelf Res.*, *26*, 132–152.

Woo, M., C. B. Pattiaratchi, and W. Schroeder (2006b), Dynamics of the Ningaloo current off Point Cloates, Western Australia, *Mar. Freshwater Res.*, *57*, 291–301.